Observing time-dependent rotational and vibrational quantum dynamics in deuterium

J. McKenna, C. R. Calvert, D. S. Murphy, J. F. McCann and I. D. Williams
Department of Mathematics and Physics, Queen's University Belfast, Belfast, BT7 1NN, UK

J. Wood, E. M. L. English and W. R. Newell
Department of Physics and Astronomy, University College London, Gower Street, London, WC1E 6BT, UK

W. A. Bryan*, I. C. E. Turcu, O. Chekhlov, K. G. Ertel, J. M. Smith and E. J. Divall
Central Laser Facility, CCLRC Rutherford Appleton Laboratory, Chilton, Didcot, Oxon., OX11 0QX, UK

R. Torres
The Blackett Laboratory, Imperial College London, Prince Consort Road, London, SW7 2BW, UK

(*also at Department of Physics and Astronomy, University College London, Gower Street, London, WC1E 6BT, UK)

Main contact email address i.williams@qub.ac.uk

Introduction

Time-resolved momentum imaging of the dynamics of small molecules using coherent optical sources is now within reach of short pulse laser science[1-3]. This area shows great promise for the control of molecular motion by an intense few-cycle laser field[4-6]. While a major drive for contemporary physics is to harness these techniques to control the reaction dynamics of large chemical and biological molecules[7], there is first a need to demonstrate the feasibility on smaller manageable and predictable systems.

The innovative idea of using coherently excited nuclear wavepackets (rotational[8-11] and vibrational[4-6]) to image and control simple molecules has recently been implemented. Enforcing such control in a systematic manner may prove revolutionary for quantum chaos[11] and information studies[9]. It has other potentially exciting applications too, particularly for molecular bond energy transfer within larger systems[5]. The quantum nature of rotational wavepackets has successfully been imaged and control has been demonstrated for some small molecules (O_2[9] and N_2[10,11]). Vibrational manipulation proves more difficult due to the faster motion of this degree of freedom although the feasibility of these experiments has been demonstrated for D_2^+[6]. We report here on an experiment on the same target molecule (D_2) where few-cycle laser pulses are used to coherently excite a superposition of D_2^+ vibrational eigenstates and subsequently to map out the wavepacket development in real-time with sub-femtosecond resolution. This motion is simulated using a quantum-mechanical approach. Likewise rotational wavepackets are also excited within this same diatomic system which are tracked as they evolve in time.

To perform the experiments a pump and probe imaging technique coupled with time-of-flight mass spectrometry is used. Although other sophisticated methods for imaging nuclear dynamics are available, for example electron rescattering-driven molecular clock[12,13], chirp of high-harmonic generation[14], this two-pulse technique provides the most flexibility for imaging the vibrational and rotational wavepacket dynamics over a long time range while maintaining high resolution. The first pulse launches the coherent D_2^+ wavepackets (see Figure 1), ionized from the neutral molecule, and the second pulse then images its development as a function of time. The system is probed via *either* the photodissociation (PD) channel through bondsoftening or above-threshold dissociation[15] leading to break-up into $D^+ + D$ fragments, *or* Coulomb explosion (CE) imaging[16] through mutual repulsion of the D^+ products. In this report we present a time-resolved observation following the dephasing and subsequent recurrence of the wavepacket structures.

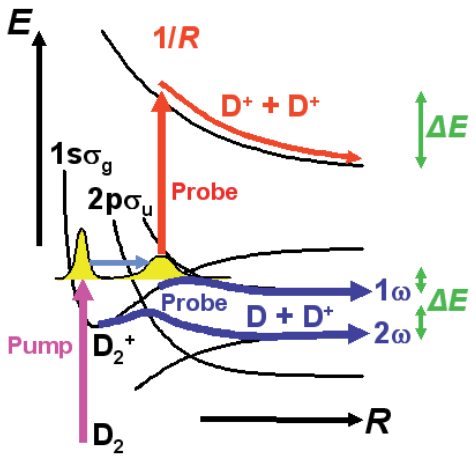

Figure 1. Schematic diagram of the pump and probe imaging technique used to map the time-resolved D_2^+ vibrational wavepacket motion. The pump pulse excites a coherent wavepacket within the molecular ion and the probe pulse images the fragmentation of the molecules as they reach the outer turning point of the potential well via the photodissociation (1ω and 2ω) or the coulomb explosion channels. These result in low and high energy fragments, respectively, which are detected through time-of-flight spectrometry. (Figure adapted from B. Feuerstein presentation)

Experimental Details

Pump and probe laser pulses were generated at the TA1 of the CCLRC RAL Astra Laser Facility. Coupling the output of a Ti:Sapphire (λ = 800 nm, $\Delta\lambda$ = 40 nm) oscillator (1 kHz rep. rate) and multipass amplifier (900 μJ output) through an argon-filled (0.3 atm) hollow-core fibre (250 μm core diameter, 1 m length), self-phase modulated spectrally broadened 700-850 nm pulses were produced. Via reflection off a set of 10 multi-layer chirped mirrors, compensating for dispersion introduced by transmission

optics and path length traversed by the beam, the pulses were compressed to few optical-cycle (10 fs) duration. A pass through a Mach-Zehnder interferometer split the beam into two components and re-overlapped them spatially enabling manipulation of their respective temporal delay with sub-fs resolution (~300 as). On-target pulses of 13 fs (40 - 50 μJ energy) measured by on line autocorrelation were used.

The interaction chamber [17] consisted of a time-of-flight (TOF) mass spectrometer (Wiley-McLaren mode) filled with spectrally-pure D_2 gas. This housed an f/5 reflective optic off which the laser pulses were focussed onto the gas target with individual peak intensities 0.8 $PWcm^{-2}$ and 0.6 $PWcm^{-2}$ for the pump and probe pulses respectively. The product ions, extracted through a 250 μm aperture by a DC electric field, were detected by a set of microchannel plates.

The small extraction aperture served to limit collection of particles to the most intense part of the laser focus and introduce a small angular acceptance to the system (half-angle 0.72°). Collection of dissociative products was therefore restricted to those fragmenting along the TOF axis or with near-thermal energy. A thin broadband λ/2 waveplate was used to orientate the polarization direction of the pump pulse perpendicular to the TOF axis while the probe pulse was naturally parallel to this axis. The reason for maintaining this directional orientation of polarization for the pulses was to ensure that any dissociation or fragmentation products from the pump pulse would go undetected due to the limited acceptance angle of the system. The probe pulse subsequently sampled those molecules aligned along the TOF axis.

Simulation of Vibrational Wavepacket Dynamics

Considering first the dynamics of the vibrational wavepacket motion, when the neutral deuterium molecule is exposed to the intense short pulse laser field it is tunnel ionized by removal of the valence electron. If this ionization process occurs over a sufficiently short time, a coherent excitation of the D_2^+ molecular ions forms a coherent superposition of vibrational eigenstates. These eigenstates form a vibrational wavepacket $|\Psi(R,t)|^2$, described by the total wavefunction:

$$\Psi(R,t) = \sum_v a_v \psi_v e^{-iE_v t/\hbar} \qquad (1)$$

for the system. Here ψ_v represents the individual wavefunctions for the vibrational eigenstates v of energy E_v, and a_v are their overlap integral with the ground $v = 0$ eigenstate of the neutral D_2 molecule following a vertical Franck-Condon (FC) transition due to the pump laser interaction. The time dependence of the system in equation (1) indicates that the vibrational wavepacket evolves in a non-stationary fashion. A plot tracking the wavepacket motion across the potential well (internuclear coordinate R) as it develops in time is shown in the probability density map in Figure 2(a). The corresponding autocorrelation function expectation value for R is shown below it in Figure 2(b).

Initially at time t = 0, the different vibrational levels are excited in phase. As a result the vibrational wavepacket is localized at small R i.e. towards the inner part of the D_2^+ potential well in Figure 1. Due to the anharmonicity of this well, the difference in energy separation between vibrational

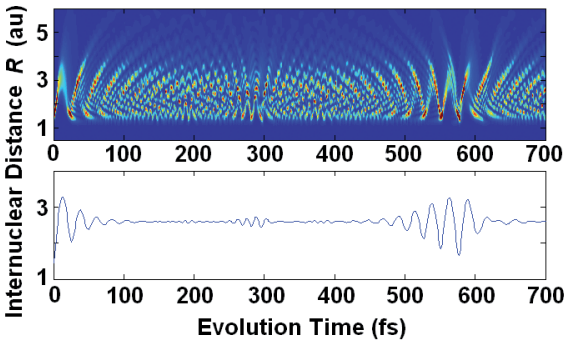

Figure 2. Quantum-mechanical simulation of the vibrational wave packet motion (a) probability density plot showing the spread of the wave packet across the internuclear coordinate R for the D_2^+ potential well as a function of time delay from production (b) expectation value $<R>$ for the wave packet.

levels gives rise to a quantum dephasing of the contributions from these states. Following a number of periods, these contributions destructively interfere, resulting in a rapid time evolution of the wavepacket, causing dissipation over a large range of R. Partial recurrences are observed when the different states are all phase shifted by multiples of π so that they constructively interfere once more creating a revival of the original wavepacket form. The first apparent reconstruction after 550 fs is in fact a half revival with the even eigenfunctions π out of phase with respect to the odd eigenfunctions [18,19]. Sub-wavepacket structures may be seen at times in between particularly after 275 fs where a miniature revival is observed.

Time-Resolved Imaging of Vibrational Dynamics

A time-resolved energy spectrum of the vibrational nuclear wavepacket motion for D_2^+ is shown in Figure 3. The two main bands of fragments at low ($0.3 < E_{frag} < 2.0$ eV) and high ($2.5 < E_{frag} < 7.0$ eV) deuteron energy are assigned to PD and CE of the molecules respectively. The revival structure predicted by the quantum-mechanical simulation is clearly visible at the expected time of 550 fs. Also visible is the initial dephasing of the wavepacket near t = 0, although in this region there is some temporal overlap of the pulses and hence the term pump and probe does strictly apply.

Experimentally ones expects to observe PD of the D_2^+ molecules (as shown in Figure 1) when the vibrational wavepacket reaches the 1ω and 3ω crossing points of the $1s\sigma_g$ and $2p\sigma_u$ potential curves. These are located at large R near the outer turning points of the well. Should the wavepacket be positioned by the inner turning point (i.e. $R \sim 1.5$ a.u.) when the probe pulse is applied, a depletion in dissociative yield is expected (provided the opening time of the dissociative gap is less than the vibrational period [20]). In this way one can track the wavepacket motion for large and small R as a function of time. At the overlap and revival regions, the location of the wavepacket is well-defined and hence the largest amplitude of oscillation in the signal is observed. Away from the revival region the wavepacket is spread unevenly across the potential well and hence one tends to observe a more constant background of PD signal.

Likewise, Coulomb explosion imaging of the wavepacket may map out its motion across the potential well if the probe pulse intensity is sufficient to bridge the large energy

gap required to reach the repulsive Coulomb state. The appearance energy of the fragments then reflects the internuclear separation when the wavepacket is lifted onto this curve ($E_{frag} \propto 1/R$). The ionization energy between the bound ($1s\sigma_g$) and repulsive Coulomb states is smallest for larger R. For the intensity of probe pulse used here (0.6 PW cm^{-2}), the majority of Coulomb explosion takes place at the larger internuclear distance. Hence instead of this mapping one tends to observe more an oscillation of the yield. However, hints of a stripe-like structure can be seen on this CE band around the time of the revival. Before the revival central time, the higher energy fragments appear at a slightly smaller delay time than the lower energy fragments mapping the wavepacket as it moves from smaller to larger R, as also apparent in Figure 2(a). After the revival centre, this structure is reversed tracking the wavepacket in the opposite direction.

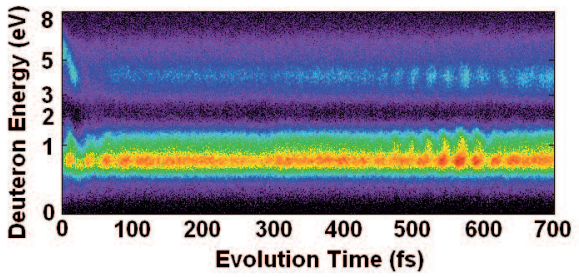

Figure 3. The kinetic energy spectra of deuterons following pump (13 fs, 0.8 PW cm^{-2}) and probe (12 fs, 0.6 PW cm^{-2}) imaging of vibrational wavepacket structure as a function of the delay between pulses. The structure centred around 550 fs is characteristic of the vibrational wavepacket revival.

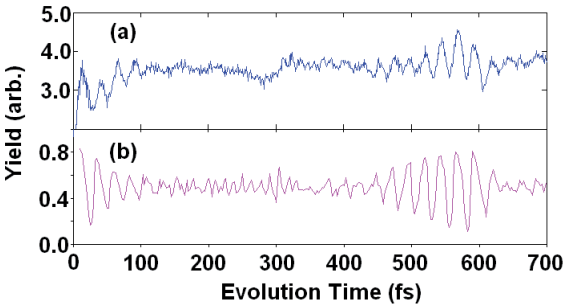

Figure 4. (a) Integrated yield of forward projected photodissociation products in the energy range 0.3 < E_{frag} < 2.0 eV from the pump-probe experiment as shown in Fig 3. and (b) Two-state calculation of the expected photodissociation yield as a function of time delay between pulses via a coupling of the $1s\sigma_g$ and $2p\sigma_u$ electronic states shown in Fig 1.

The oscillation period of the peak structure in the revival region is measured as 21 fs which agrees well with the classical vibrational period for the lowest vibrational states of D_2^+ and with the quantum mechanical simulation in Figure 2(a). To clearly resolve this structure, the experimental resolution limited by the pulse length, must be sufficient. Perhaps this explains why the mini-revival structure around 300 fs, predicted by the simulation, is not observed. In this region the vibrational wavepacket is split into two sub-wavepackets which oscillate out of phase by half the vibrational period. The characteristic oscillation period for the half cycle is therefore 10.5 fs. Since the pulse duration of the pump and probe pulses used in this experiment were 13 fs and 12 fs respectively, one should not expect to be able to resolve these features.

To obtain a direct measure of the expected PD yield as a function of time, a coupling of the $1s\sigma_g$ and $2p\sigma_u$ states has been introduced in an extension to the simulation to allow for the transfer of population between these levels in the presence of the probe pulse. Pulse parameters similar to those in the experiment are used. This numerical model is a full one-dimensional, two-state, wavepacket simulation in the presence of the probe pulse, with individual simulations carried out for each value of the delay time. It is performed by way of an eight-order Taylor series propagator method with the vibrational wavepacket represented on a finite-difference grid in internuclear coordinate space, R.

The results from the calculation are shown in Figure 4(b). In the upper panel, Figure 4(a), the corresponding integrated yield as a function of time delay from the experimental data of Figure 3 for the low energy ($0.3 < E_{frag} < 2.0$ eV) PD fragments is shown. These two plots are directly comparable. While the amplitude of the experimental revival oscillation is much reduced by comparison to the calculation, the overall features are strikingly similar. In both the experiment and the theory the revival structure appears as a slow build up in the oscillation which rapidly dampens shortly after the wavepacket has been fully reconstructed. The source of this effect has been tested by switching *on* and *off* active vibrational levels in the simulation and it is found that this asymmetry in the revival is highly sensitive to the inclusion of the high lying vibrational levels ($v > 10$). The revival is symmetric about its central time should these states be omitted. This reflects the increasing anharmonicity of the D_2^+ potential well as one moves towards the continuum. The need to include these states to reproduce the experimental results helps to affirm the assignment of a FC transition due to the short pump pulse. Indeed the sensitivity of the revival structure to the vibrational population suggests that it may be used as a diagnostic tool reflecting the vibrational distribution of the states involved.

Rotational Wavepackets

Just as a vibrational wavepacket is set up by exciting a range of vibrational states in D_2^+ which subsequently interfere (constructively and destructively) as a function of time, a rotational wavepacket is created in the same way. The pump laser pulse acts to populate a range of the different rotational states of the molecule, i.e. states of different J quantum number. From a classical point of view, one may consider the molecule as a rigid rotor. The impulse of the laser field, with its polarization direction orientated along a particular direction, induces a dipole moment in the molecule and acts to pull the molecule into alignment with the directional vector of the E-field. As the pulse duration of the laser is short compared to the characteristic rotation time of the molecule, the molecule continues to rotate (diabatically) in the field-free time when the laser impact is over. Like the vibrational levels, the rotational levels are also situated in an anharmonic potential (with a higher degree of anharmonicity). The individual J states therefore have different classical rotation times due to the unequal spacing of the energy levels. Rotational revivals are observed when the states are

all in phase with one another which repeats at the fundamental frequency for the system ($\pi\hbar/B_e$).

The rotational wavepacket induced by the laser interaction may be simulated by considering a coherent superposition of the rotational states[21]. This may be written as:

$$\Phi(R,t) = \sum_J a_J \phi_J e^{-iE_J t/\hbar} \qquad (2)$$

The coefficients a_J are determined by the interaction of the laser pulse with the molecules, ϕ_J are the eigenfunctions for the rotational J states and E_J the corresponding energy. The eigenfunctions for the system are the spherical harmonics with the angular dependence θ defined with respect to the polarization axis of the aligning pulse. A measure of the degree of alignment within the molecular sample at any given time t is defined by the expectation value $\langle\cos^2\theta\rangle$. When considering an ensemble of molecules in thermal equilibrium as for the experiment here, this value must be averaged over the initial Boltzmann distribution of J states.

In Figure 4 this alignment parameter is plotted for a 12 fs laser pulse interacting with a sample of D_2 molecules at T = 300 K. The background level for the $\langle\cos^2\theta\rangle$ parameter is 0.33 corresponding to an isotropic distribution of the molecules within the sample. An increase in this value indicates a larger degree of alignment to the electric field vector direction while a decrease corresponds to a greater degree of anti-alignment. The alignment is highly sensitive to the pulse intensity used. The first full rotational revival appears at a time on the order of 550 fs with a fractional revival structure after 275 fs.

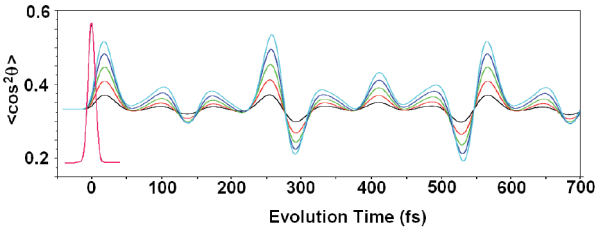

Figure 5. Quantum-mechanical simulation of the rotational wave packet motion induced in target D_2 molecules at 300 K as a function of time. The alignment parameter $\langle\cos^2\theta\rangle$ is given with θ measured with respect to the aligning pulse polarization vector. The various coloured curves are for an aligning pulse, centred at t = 0 (pink), with intensites ranging from 0.1 PW cm^{-2} (black) to 0.5 PW cm^{-2} (light blue) in integer steps.

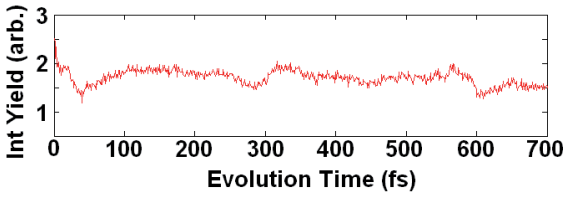

Figure 6. Integrated yield from the Coulomb explosion imaging of rotational wavepacket structure from D_2 target molecules as a function of time. Pump (14 fs, 0.6 PW cm^{-2}) and probe (14 fs, 0.4 PW cm^{-2}) laser pulses were used.

The geometry of the time-of-flight configuration used for the experiments here, i.e. a small angular acceptance along the detector axis, ensures selective imaging of only those molecules aligned along this direction. The experiments are therefore sensitive to the rotational degree of alignment. Although there are signatures of rotational structure in Fig 4(a), particularly centred around 300 fs and underlying the peaks at 600 fs, it has largely been masked by the vibrational structure at this time. Plotted in Figure 5 is the integrated yield of the CE signal ($2.5 < E_{frag} < 7$ eV) from a pump-probe experiment similar to that of Figure 3 but with slightly differing conditions (pump: 14 fs, 0.6 PW cm^{-2}, probe: 14 fs, 0.4 PW cm^{-2}). While the alignment parameter $\langle\cos^2\theta\rangle$ in the simulation is given for θ measured with respect to the pump pulse polarization direction, in the experiment this direction is orthogonal to the detector axis. As a result, peaks in the simulation corresponding to maximum alignment appear as troughs in the experiment where the molecules are aligned perpendicular to the detector axis and hence go undetected. Vice versa for the minima in the $\langle\cos^2\theta\rangle$ parameter. The results from the simulation agree well this the experimental data predicting the expected time for the rotational revival structure and the main overall features.

Conclusion

Using two pulse pump and probe imaging with few cycle laser pulses, we have successfully mapped out both the vibrational and rotational structure of the simple diatomic system, D_2^+, which is of fundamental interest to the community. The characteristic dephasing and revival of the set of quantum vibrational/rotational states has been observed, and is found to concur well with quantum-mechanical simulations of their, respective, wavepacket motion. Both the vibrational and rotational structure have been successfully described independently, using pure vibration/rotation models, without the need to invoke a rovibrational quantum wavepacket.

References

1. F. Legare *et al.*, *Phys. Rev. A* **72** 052717 (2005).
2. A. S. Alnaser *et al.*, *Phys. Rev. A* **72** 030702(R) (2005).
3. Th. Ergler *et al.*, *J. Phys. B* **39** S493 (2006).
4. H. Niikura *et al.*, *Phys. Rev. Lett.* **90** 203601 (2003).
5. H. Niikura *et al.*, *Phys. Rev. Lett.* **92**, 133002 (2004).
6. H. Niikura *et al.*, *Phys. Rev. A* **73** 021402(R) (2006).
7. A. H. Zewail, *J. Phys. Chem.* **104** 5660 (2000).
8. C. Z. Bisgaard *et al.*, *Phys. Rev. Lett.* **92**, 173004 (2004).
9. K. F. Lee *et al.*, *Phys. Rev. Lett.* **93**, 233601) (2004).
10. M. Renard *et al.*, *Phys. Rev. A* **72**, 025401 (2005).
11. K. F. Lee *et al.*, *Phys. Rev. A* **73**, 033403(R) (2006).
12. H. Niikura *et al.*, *Nature* **417** 917 (2002).
13. H. Niikura *et al.*, *Nature* **421** 826 (2003).
14. S. Baker *et al.*, *Science* **312** 424 (2006).
15. P. H. Bauksbaum *et al.*, *Phys. Rev. Lett.* **64** 1883 (1990).
16. W. A. Bryan *et al.*, *J. Phys. B* **33** 745 (2000).
17. H. Stapelfeldt *et al.*, *Phys. Rev. A* **58** 426 (1998).
18. I. Sh. Averbukh and N. F. Perelman, *Phys. Lett. A* **139** 449 (1989).
19. Vrakking *et al.*, *Phys. Rev. A* **54** R37 (1995).
20. J. Wood *et al.*, *CCLRC RAL Annual Report (2006)*.
21. R. Torres *et al.*, *Phys. Rev. A* **72** 023420 (2005).